Shallow Moist Convection

T. Weidauer[1], C. Junghans[2], O. Pauluis[3], M. Pütz[2], and J. Schumacher[1]

[1] Institute of Thermodynamics and Fluid Mechanics, Technische Universität Ilmenau
D-98684 Ilmenau, Germany
E-mail: joerg.schumacher@tu-ilmenau.de

[2] Deep Computing – Strategic Growth Business, IBM Deutschland GmbH
D-55131 Mainz, Germany

[3] Center for Atmosphere Ocean Science, New York University
New York City, NY 10012-1185, USA

Convective turbulence with phase changes and latent release is an important dynamical process in the atmosphere of the Earth which causes, e.g. the formation of clouds. Here we study moist convection in a simplified setting – shallow and nonprecipitating moist Rayleigh-Bénard convection with a piecewise linear thermodynamics on both sides of the phase boundary. The presented model is a first nontrivial extension of the classical dry Rayleigh-Bénard convection. The equations of motion and linear stability studies of equilibria are discussed and supercomputations of the fully developed turbulent dynamics in very flat Cartesian cells are presented.

1 Introduction

Moist thermal convection combines turbulent convection with phase changes and latent heat release. It is ubiquitous throughout the atmosphere of the Earth[8]. When a parcel of air rises in convective motion, it expands adiabatically. As a consequence, its temperature and pressure drop and at some point during its ascent the air parcel becomes saturated. The water condensation sets in and clouds are formed. The large range of temporal and spatial scales in the convective turbulent motion causes big variations in the lifetime and shape of clouds, such as shallow stratocumulus or isolated cumulus clouds, and thus in the cloud cover and radiation budget. Cloud parametrizations remain therefore one of the big uncertainty factors for global circulation and climate models[8].

Despite its enormous importance, the small-scale structure and statistics of moist convective turbulence has been studied relatively little compared to its dry convection counterpart. The reason for this gap is that turbulent convection in moist air includes the complex nonlinear thermodynamics of phase changes in addition to the turbulent motion[2,14]. Phase changes lead to discontinuities of the partial derivatives in the equation of state at the saturation point[6]. The associated latent heat release in the bulk provides a rapidly changing local source of buoyant motion, in addition to the buoyancy (or heat) flux from the bottom to the top planes as already present in dry convection. Significant progress in understanding the global and local mechanisms of turbulent heat transfer in dry convection has been made in the last decade (for a comprehensive review see Ref. 1).

In this work, we aim at transfering the numerical analysis concepts from the well-investigated dry convection case[1,7,11,12] to the less-explored moist convection case. We make a first step by considering moist Rayleigh-Bénard convection with a linearized thermodynamics of phase changes[9]. The model is a straightforward extension of the well-known dry Rayleigh-Bénard convection case in the Boussinesq approximation[11,12]. It is

also an extension of a moist convection model which was discussed originally by Bretherton[4,5] for the onset of linear instability and weakly nonlinear regime. Here, we conduct direct numerical simulations of the turbulent nonlinear stage of moist convection and discuss the computational challenges for studies in flat cells[10].

2 Moist Boussinesq Model

2.1 Thermodynamic Equilibrium Approximation for a Shallow Layer

The buoyancy B in atmospheric convection is given by[6]

$$B = -g\frac{\rho(S, q_v, q_l, q_i, p) - \overline{\rho}}{\overline{\rho}}\,, \tag{1}$$

with g being the gravity acceleration, $\overline{\rho}$ a mean density, p the pressure, S the entropy and q_v, q_l, q_i the mixing ratios of water vapor, liquid water and ice. So-called warm clouds result in $q_i = 0$. If we assume local thermodynamic equilibrium, which means for example that precipitation is absent, the two remaining mixing ratios are combined to the total water mixing ratio, $q_T = q_v + q_l$. Thus dependencies are reduced to $B(p, S, q_T)$. The Boussinesq approximation considers pressure variations about a mean hydrostatic profile and thus one is left with a function $B(S, q_T, z)$. However, this functional dependence is still highly nonlinear and contains the full thermodynamics of phase changes. The next step is to approximate B as a piecewise linear function of S and q_T for both phases (vapor and liquid) close to the phase boundary. This step preserves the main new physical ingredient, the discontinuity of partial derivatives (e.g. the specific heat) at the phase boundary, but allows for an explicit determination of whether the air is locally saturated or not. Since B becomes a linear function of S and q_T, we can introduce two new prognostic buoyancy fields, a *dry buoyancy field* D and a *moist buoyancy field* M, which substitute S and q_T. Consequently, the buoyancy $B(M, D, z)$ is a linear function of M and D and is given at each space-time-point by

$$B = \max\left(M, D - N_s^2 z\right)\,, \tag{2}$$

where N_s is the Brunt-Vaisala frequency. An air parcel at position $\mathbf{x}$ at time t is unsaturated if $M(\mathbf{x}, t) < D(\mathbf{x}, t) - N_s^2 z$; it is saturated if $M(\mathbf{x}, t) > D(\mathbf{x}, t) - N_s^2 z$.

2.2 Equations of Motion and Dimensionless Parameters of the Model

The dry and moist buoyancy fields can be decomposed in a linear mean and variations about the mean

$$D(\mathbf{x}, t) = \overline{D}(z) + D'(\mathbf{x}, t) = D_0 + \frac{D_H - D_0}{H} z + D'(\mathbf{x}, t) \tag{3}$$

$$M(\mathbf{x}, t) = \overline{M}(z) + M'(\mathbf{x}, t) = M_0 + \frac{M_H - M_0}{H} z + M'(\mathbf{x}, t)\,. \tag{4}$$

The variations about the mean profiles of both fields have to vanish at $z = 0$ and H, which imposes the boundary conditions $D' = 0$ and $M' = 0$. Eq. (2) can now be transformed into $B = \overline{M}(z) + \max\left(M', D' + \overline{D}(z) - \overline{M}(z) - N_s^2 z\right)$. Note that the first term on the right-hand side is horizontally uniform. This implies that it can be balanced by a horizontally

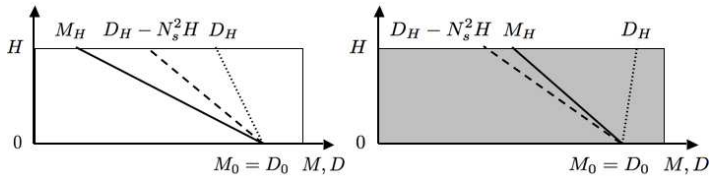

Figure 1. Left: Completely unsaturated intital equilibrium condition with $\overline{M}(z) < \overline{D}(z) - N_s^2 z$. Both buoyancy fields are linearly unstable for sufficiently high Rayleigh numbers. Right: Conditionally unstable equilibrium case. The dry buoyancy field is linearly stable. The whole slab is saturated and $\overline{M}(z) > \overline{D}(z) - N_s^2 z$. D_0, M_0, D_H and M_H are prescribed values of both fields at $z = 0$ and H.

uniform pressure field given by $p(z) = -M_0 z - [(M_H - M_0)/(2H)]z^2$. We can thus remove the mean contribution from the buoyancy field without any loss of generality.

A dimensionless version of the equations of motion is obtained by defining the characteristic quantities. These are the height of the layer H, the free-fall velocity $U_f = \sqrt{H(M_0 - M_H)}$, the time $T_f = H/U_f$, the characteristic (kinematic) pressure U_f^2, and the characteristic buoyancy difference $M_0 - M_H$. The Boussinesq equations are given by

$$\frac{\partial \mathbf{u}}{\partial t} + (\mathbf{u} \cdot \nabla)\mathbf{u} = -\nabla p + \sqrt{\frac{Pr}{Ra_M}} \nabla^2 \mathbf{u} + B(M, D, z)\mathbf{e}_z \tag{5}$$

$$\nabla \cdot \mathbf{u} = 0 \tag{6}$$

$$\frac{\partial D'}{\partial t} + (\mathbf{u} \cdot \nabla)D' = \frac{1}{\sqrt{PrRa_M}} \nabla^2 D' + \frac{Ra_D}{Ra_M} u_z \tag{7}$$

$$\frac{\partial M'}{\partial t} + (\mathbf{u} \cdot \nabla)M' = \frac{1}{\sqrt{PrRa_M}} \nabla^2 M' + u_z \tag{8}$$

We identify three non-dimensional parameters: the Prandtl number, Pr, the dry and the moist Rayleigh numbers, Ra_D and Ra_M, which are defined as

$$Pr = \frac{\nu}{\kappa}, \qquad Ra_D = \frac{H^3(D_0 - D_H)}{\nu\kappa}, \qquad Ra_M = \frac{H^3(M_0 - M_H)}{\nu\kappa}\,. \tag{9}$$

The kinematic viscosity is ν and the diffusivity of the buoyancy fields is κ. Two more parameters are hidden implicitly within the definition (2) of the buoyancy B which is given in dimensionless form by

$$B = \max\left(M', D' + SSD + \left(1 - \frac{Ra_D}{Ra_M}\right) z - CSAz\right)\,. \tag{10}$$

The so-called *Surface Saturation Deficit* SSD and the *Condensation in Saturated Ascent* CSA are defined as

$$SSD = \frac{D_0 - M_0}{M_0 - M_H}\,, \qquad CSA = \frac{N_s^2 H}{M_0 - M_H}\,. \tag{11}$$

These two new non-dimensional parameters respectively measure how close the lower boundary is to be saturated, and how much water can condense within the shallow layer. When $D_0 - M_0$ is positive, the air at the lower boundary is unsaturated, and $D_0 - M_0$ is

Run	iproc	jproc	T_{P3DFFT}	$T_{PB3DFFT}$	Speedup
1	64	32	10910 secs	10829 secs	$\sim 1\%$
2	64	64	7301 secs	7127 secs	2%
3	128	64	6934 secs	5585 secs	19%

Table 1. Runtime tests on Blue Gene/P for the full moist convection code in production mode on a $2048 \times 2048 \times 513$ grid. The number of MPI tasks is iproc×jproc. Integration was done for 300 time steps.

the amount of water vapor that must be added to an air parcel to become saturated. For convection over the ocean, the lower boundary can just be saturated, i.e. $SSD = 0$. In the following we will consider a three-dimensional subspace of the five-dimensional parameter space only. We will restrict the present study to $Pr = 0.7$ and $SSD = 0$.

2.3 Numerical Scheme and Computational Challenges

We solve the model equations in a flat Cartesian slab with $L_x = L_y = \Gamma H$ with $\Gamma \gg 1$ being the aspect ratio. In the lateral direction we apply periodic boundary conditions, in the vertical direction free-slip boundary conditions. They are given by

$$u_z = D' = M' = 0 \quad \text{and} \quad \frac{\partial u_x}{\partial z} = \frac{\partial u_y}{\partial z} = 0 \tag{12}$$

at $z = 0, H$. The equations of motion are solved by a pseudospectral scheme with volumetric fast Fourier transformations (FFT) and 2/3 de-aliasing. Time-stepping is done by a second-order Runge-Kutta scheme. The smallest resolved scale is the Kolmogorov dissipation length which limits the Rayleigh numbers of our DNS to values of $\sim 10^8$. We use B' in the momentum Eq. (5) instead of B since the mean contribution is $\overline{B}(z)$ and can be added to the kinematic pressure, i.e. $\partial_z p + B = \partial_z \tilde{p} + B'$.

Convection in flat and highly resolved Cartesian cells with grid point numbers $N_x = N_y \gg N_z$ causes challenges for a parallel implementation of the code. On the one hand, massively parallel computers are necessary to process such problem at hand. On the other hand, the geometry requires a two-dimensional parallelization, i.e. the volume $V = \Gamma H \times \Gamma H \times H$ has to be decomposed into iproc×jproc pencils each associated with a MPI task[10]. The resulting volumetric FFTs have to be highly scalable, i.e. increasing the number of CPUs to solve the problem should also substantially decrease the time-to-answer. Recall that three-dimensional FFTs require several global communication steps across the full processor grid. In our code, the FFTs in total consume 87% of the computing time. We compared here two code versions with three-dimenional FFT packages, the P3DFFT-package by D. Pekurovsky[15] and an improved package PB3DFFT with a cache blocking such that the data portions fit into the fast L2 cache of the processors. This avoids several reloadings into L2 during execution of the FFTs along the three coordinate directions and causes a slight speed-up in some cases. In Table 1, we report a test series of runs for $\Gamma = 4$. Although the listed results look promising further efforts of improvement are under way, in particular for very flat cells with $\Gamma = 16$ or 32. The MPI task mapping on the 3d Torus in Blue Gene/P becomes then more and more essential. It should be stated that cache blocking works significantly better on POWER-6 systems where 8 times more memory per core is available than on Blue Gene/P.

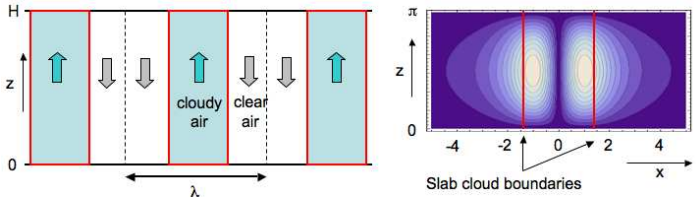

Figure 2. Left: Sketch of the configuration in a conditionally unstable layer that can be solved analytically. Red lines are the cloud boundaries where matching conditions have to be satisfied. The arrows indicate up- and downwelling air. Right: Contours of the velocity stream function which correspond with streamlines of the 2D velocity field of a linearly unstable mode. The parameters are $Ra_M = 3409$, $Ra_D = -955$ and $Pr = 0.7$. The periodicity length is $\lambda \to \infty$. The growth rate is $\Omega = 0.2485$, $t = 0.1$ and $\gamma = 2.8$.

3 Linear Stability of a Shallow Moist Convection Layer

Case of $Ra_D > 0$ and $Ra_M > 0$: Starting point of our dynamical studies is an equilibrium configuration which is infinitesimally perturbed and evolves into a fully developed turbulent state. The equilibrium configuration for a convection layer is a fluid at rest ($\mathbf{u} = 0$) and linear profiles of both buoyancy fields, $\overline{D}(z)$ and $\overline{M}(z)$ as defined in Eq. (3) and (4). In case that both Rayleigh numbers are positive, the linear instability sets in at a critical value[6], i.e. Ra_D and $Ra_M > Ra_c = 27\pi^4/4 \approx 657.5$. Under most circumstances, the amount of water in the atmosphere decreases with height. This implies that the moist Rayleigh number should be larger than the dry Rayleigh number, $Ra_M \geq Ra_D$ (see Figure 1, left).

Case of $Ra_D < 0$ and $Ra_M > 0$: In the atmosphere, another situation is often present. An air parcel is unstable if it is saturated, but stable if it is unsaturated. In case of saturation condensation sets in which is connected with a local release of latent heat and an upward motion of the parcel. We call this regime *conditional instability*[3,6]. In this case, the dry Rayleigh number $Ra_D < 0$, which is sketched in Figure 1 (right). The particular case of $\overline{M}(z) = \overline{D}(z) - N_s^2 z$ was discussed in a closely related model by Bretherton[4,5]. He was able to progress for the two-dimensional case (no y-dependence of all fields) along the same lines as a classical linear stability analysis of dry convection. For the onset of linear instability a periodic slab cloud configuration, as sketched in Figure 2 (left), will be obtained. Moist cloudy air is rising up inside the slab clouds and clear air is falling down outside. Since $\overline{M}(z) = \overline{D}(z) - N_s^2 z$, one needs to discuss one buoyancy field only, M'. The partial derivatives are discontinuous at the cloud boundary and thus additional matching conditions in x direction have to be satisfied. This prohibits a normal mode ansatz in x. With the moist potential, $L(x,z,t) := \int M'(x,z,t)\mathrm{d}x$, Bretherton ended up at a 6th-order ordinary differential equation

$$\left[Ra_M \frac{\partial^2}{\partial t^2}\nabla^2 - \left(\sqrt{\frac{Ra_M}{Pr}} + \sqrt{PrRa_M} \right) \nabla^4 \frac{\partial}{\partial t} + \nabla^6 \right] L = R \frac{\partial^2}{\partial x^2} L \,, \qquad (13)$$

with $R = Ra_M$ if $M'(x,z,t) > 0$ and $R = Ra_D$ otherwise. The free-slip boundary conditions are given by $L = \partial^2 L/\partial z^2 = \partial^4 L/\partial z^4 = 0$ for $z = 0, H$. The matching conditions in x result in six relations $\partial^n L/\partial x^n = 0$ for $x = \pm\gamma/2$ where $n = 0, ..., 5$. The separation ansatz $L(x,z,t) = \exp(\Omega t) G(x) \sin(\pi z/H)$ is now used where $G(x + n\lambda) = G(x)$, as

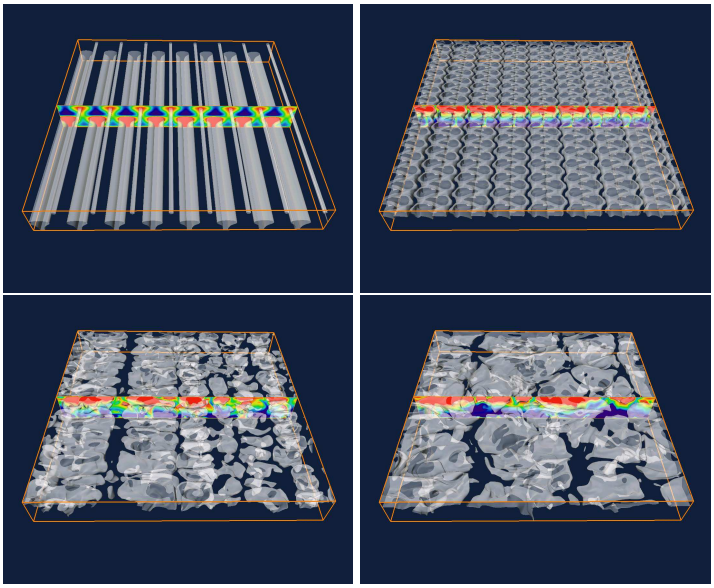

Figure 3. Evolution of clouds from the initial equilibrium configuration to the fully developed turbulent state. Times are $t/T_f = 11.9$ (top left), $t/T_f = 41.6$ (top right), $t/T_f = 64.0$ (bottom left) and $t/T_f = 96.7$ (bottom right). Isosurfaces of the cloud boundary and a two-dimensional contour slice of q_l are shown. Here, $CSA = 0.35$, $Ra_D = 7.0 \times 10^5$, $Ra_M = 1.4 \times 10^6$ and $\Gamma = 8$.

shown in Figure 2 (left). Solutions G in dry and moist areas have to be matched at yet not known cloud boundary positions $x = \pm\gamma/2$. Figure 2 (right) shows an example of the flow field triggered by the linear instability for an isolated cloud with $\lambda \to \infty$. The slab of cloudy air tends to become narrower than the dry air regions surrounding it, as already shown in a simple model by Bjerknes[3].

4 Numerical Simulations of the Full Turbulent Regime

Case of $Ra_D > 0$ *and* $Ra_M > 0$: Our numerical computations of the fully developed turbulent regime were mostly focused so far on the case where both buoyancy fields are linearly unstable. An initial equilibrium configuration is perturbed infinitesimally. After a transient phase of $t/T_f \sim 10^2$, the convective flow is relaxed into a statistically stationary state. This evolution is illustrated by the four snapshots in Figure 3. An important aspect of the simulations is the evolution of the cloud patterns. Clouds are defined in our model as the space-time regions with a liquid water mixing ratio $q_l(\mathbf{x}, t) = M(\mathbf{x}, t) - (D(\mathbf{x}, t) - N_s^2 z) \geq 0$. Our parametric studies found that the size of the cloud patterns depends on both, the parameter CSA and the two Rayleigh numbers Ra_D and Ra_M. The covering of the layer by clouds is decreased with increasing Rayleigh numbers. Furthermore, the larger CSA the more water can be condensed during an adiabatic ascent. A decrease of this parameter allows to study a transition from a closed cloud layer to a broken one. Figure 4 shows an example with a small cloud cover[13]. Isolated clouds are found in regions where air is rising up from the ground (red isosurfaces). The

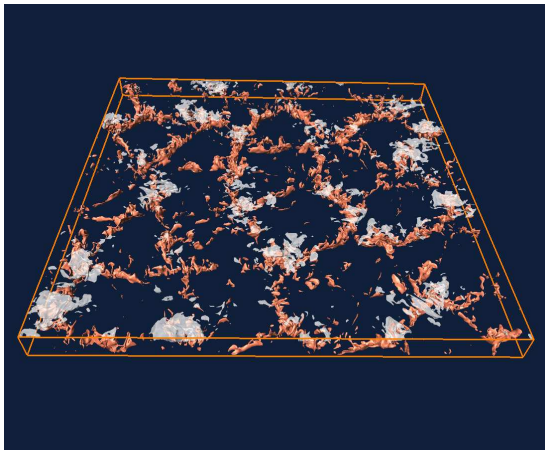

Figure 4. Snapshot of a turbulent shallow convection layer. The cell with an aspect ratio of 16 is resolved by $2048 \times 2048 \times 129$ grid points. The simulation was run on one Blue Gene/P rack (4096 MPI tasks) and took 10 days. The red isocontours show upwelling motion with $u_z \geq 0.23 U_f$. Right above this skeleton of upwelling fluid, clouds are formed which are displayed as grey transparent isosurfaces.

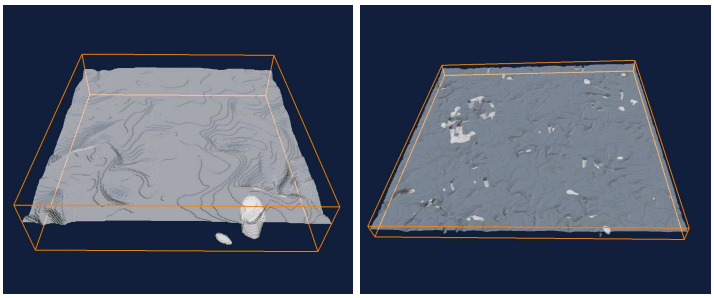

Figure 5. Cloud base isosurface for moist convection in a conditionally unstable layer. The numbers here, $Ra_D = -1.0 \times 10^5$ and $Ra_M = 2.5 \times 10^5$. Left: $\Gamma = 4$. Right: $\Gamma = 16$. Clouds fill the whole slab above the isosurface.

perimeter-area analysis of vertically averaged cloud distribution gave a scaling dimension of 1.27 which is close to 1.32 from large eddy simulations of cumulus convection.

Case of $Ra_D < 0$ and $Ra_M > 0$: In the case of conditional instability, we applied a finite perturbation to a configuration sketched in Figure 1 (right) in order to overcome the stabilizing effect of the dry buoyancy field. Note that this initial configuration differs from the slab cloud ansatz (see Figure 2 (right)) in the linear stability analysis of Bretherton. Our first studies indicate that this regime is very sensitive to the aspect ratio Γ and the amplitude of the perturbation (not shown here). This is illustrated in Figure 5 for $\Gamma = 4$ and $\Gamma = 16$. The cloud base, $q_l = 0$, is shown for snapshots of the turbulent states. Scattered across the nearly unbroken cloud layer are cloud pieces that reach down to the bottom layer. They reproduce the feature which was illustrated in Figure 2. We see also that their number grows with Γ since the system gains a bigger variability to compensate upwelling moist air by downwelling dry air.

In summary, we have shown that the present model can display several features of moist convection. It is thus an appropriate base for the investigation of the impact of phase changes and latent heat release on the turbulence and vice versa. The model allows to include further effects such as rotation of the plane or more importantly radiative cooling at the top.

Acknowledgements

The computer time on the Blue Gene/P system JUGENE at the Jülich Supercomputing Centre (Germany) was provided by the DEISA grant "Cloud09" and by grant HIL02. JS wishes to thank Florian Janetzko for his help and acknowledges support by the DFG. OP is supported by the NSF.

References

1. G. Ahlers, S. Grossmann and D. Lohse, *Heat transfer & large-scale dynamics in turbulent Rayleigh-Bénard convection*, Rev. Mod. Phys. **81**, 503-537, 2009 .
2. P. R. Bannon, *Theoretical foundations for models of moist convection*, J. Atmos. Sci. **59**, 1967-1982, 2002.
3. J. Bjerknes, *Saturated-adiabatic ascent of air through dry adiabatically descending environment*, Quat. J. R. Met. Soc. **64**, 325-330, 1938.
4. C. S. Bretherton, *A theory for nonprecipitating moist convection between two parallel plates. Part I: Thermodynamics and "linear" solutions*, J. Atmos. Sci. **44**, 1809-1827, 1987.
5. C. S. Bretherton, *A theory for nonprecipitating moist convection between two parallel plates. Part II: Nonlinear theory and cloud field organization*, J. Atmos. Sci. **45**, 2391-2415, 1988.
6. K. A. Emanuel, *Atmospheric convection*. Oxford University Press, Oxford, 1994.
7. M. S. Emran and J. Schumacher, *Fine-scale statistics of temperature and its derivatives in convective turbulence*, J. Fluid Mech. **611**, 13-34, 2008.
8. J. Heintzenberg and R. J. Charlson, *Clouds in the Perturbed Climate System*. Strüngmann Forum Reports, MIT Press, Cambridge, Massachusetts, 2009.
9. O. Pauluis and J. Schumacher, *Idealized moist Rayleigh-Bénard convection with piecewise linear equation of state*, Comm. Math. Sci. **8**, 295-319, 2010.
10. J. Schumacher and M. Pütz, *Turbulence in laterally extended systems*, in Proc. of the International Conference ParCo 2007, Editors: C. Bischof, M. Bücker, P. Gibbon, G. Joubert, T. Lippert, B. Mohr und F. Peters, NIC Series 38, Jülich 2007, 585-592 (2007).
11. J. Schumacher, *Lagrangian dispersion and heat transport in convective turbulence*, Phys. Rev. Lett. **100**, 134502 (4 pages), 2008.
12. J. Schumacher, *Lagrangian studies in convective turbulence*, Phys. Rev. E **79**, 056301 (13 pages), 2009.
13. J. Schumacher and O. Pauluis, *Buoyancy statistics in moist turbulent Rayleigh-Bénard convection*, J. Fluid Mech., in press, 2010.
    `http://arxiv.org/abs/0912.5195`.
14. B. Stevens, *Moist convection*, Annu. Rev. Earth Planet. Sci. **33**, 605-643 (2005).
15. `http://www.sdsc.edu/us/ressources/p3dfft.php`.